Probing of Optically Responsive Paramagnetic Ions via Light-Intensity-Modulated EPR

Ji-Min Song, [a] Qing-Song Deng, [b] Jia-Xin Chen, [a] Yu-Qian Liu, [a] Geng-Yuan Li, [a] Song Gao, [a, b, c] Ye-Xin Wang, [# d] Zheng Liu, [# b] Shang-Da Jiang [# a]

Content of Supplementary Information

1. Simulation of the MFM-EPR Spectrum for Ce:YAG

Based on the simulation of the single-crystal rotation spectra of Ce:YAG (Figure S1), we determined that the angle between the [100] axis of the Ce:YAG crystal and the external magnetic field (B_0) in the LIM CW-EPR experiment is 22°.

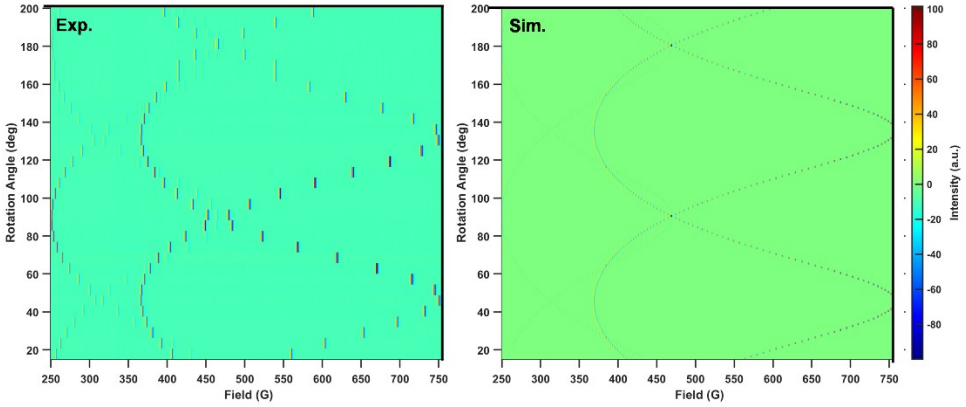

Figure S1. Angle-dependent CW-EPR spectra of CeYAG measured at 15 K (left) and the corresponding simulation (right). The rotation axis is <001>.

2. Signal Characteristics of LIM CW-EPR vs. MFM-EPR

We further elucidate the fundamental difference in spectral features between conventional Magnetic Field Modulation (MFM) and the Light Intensity Modulation (LIM) technique developed in this study. As illustrated in Figure S2, the raw EPR response of a paramagnetic system typically manifests as an absorption profile (Figure S2a). In conventional MFM CW-EPR, detection relies on a small-amplitude AC magnetic field superimposed on the static field B_0. This modulation periodically shifts the resonance condition, effectively probing the slope of the absorption curve. Consequently, the signal extracted via lock-in detection corresponds to the first derivative of the absorption line shape, resulting in the characteristic derivative peak shown in Figure S2b.

In contrast, the LIM technique employs a fundamentally different modulation mechanism. Instead of perturbing the energy level splitting via the magnetic field, LIM utilizes periodic laser switching to modulate the population difference (ΔN) between the spin sublevels at a fixed magnetic field. Laser excitation drives the system away from thermal equilibrium, while relaxation processes restore it, causing the population difference—and thus the microwave absorption—to oscillate at the modulation frequency. Since the lock-in amplifier in this configuration detects the amplitude of these population-induced absorption changes rather than the slope of the resonance condition, the demodulated LIM signal retains the original absorption peak profile, as depicted in Figure S2c. This distinction confirms that the LIM signal directly reflects

the steady-state response of the spin population under optical pumping, rather than the field-gradient sensitivity inherent to MFM.

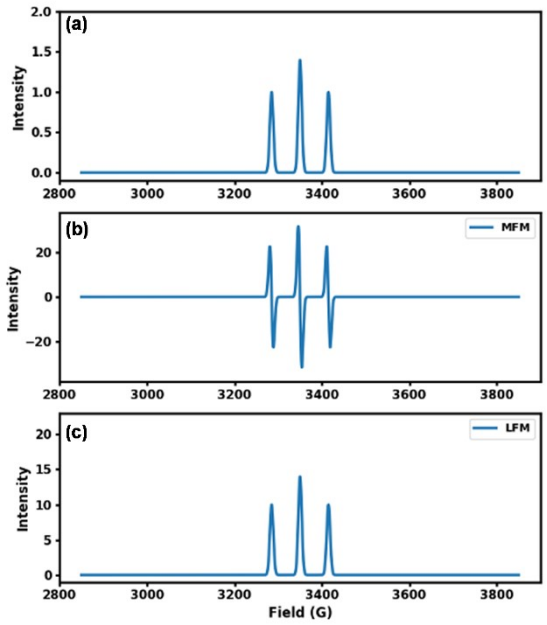

Figure S2. Schematic comparison of the signal features between MFM CW-EPR and LIM CW-EPR. (a) The microwave absorption peak of the spin system without modulation or phase-sensitive detection. (b) Typical first-derivative spectrum obtained via MFM. (c) Absorption-type spectrum obtained via LIM.

3. Theoretical Modeling: Four-Level System and Rate Equations

The spin dynamics of the Ce:YAG system are quantitatively described by the following equations, which govern the time evolution of the populations in the ground-state doublet ($^{G_\alpha}$ and $^{G_\beta}$), the 5d excited state (^{E}), and the intermediate metastable states (^{M}). In this model, the thermal equilibrium between the ground-state spin sublevels is determined by the Boltzmann factor, denoted as *P*. Accordingly, the spin-lattice relaxation rate $^{k_{T_1}}$ is defined as $^{k_{T_1} = 1/T_1}$, where ^{T_1} is the spin-lattice relaxation time of the ground spin sublevels. By solving this set of differential equations, the population difference (ΔN) can be obtained, which ultimately manifests as the signal intensity. Figure S3 displays the simulated time-domain signal based on the model at 15K, with a modulation frequency of 5 kHz and a duty cycle of 50%.

$$\frac{d[E]}{dt} = k_l \cdot ([G_\alpha] + [G_\beta] + [M]) - (k_{E\to G} + k_{E\to M}) \cdot [E] \#(S1)$$

$$\frac{d[M]}{dt} = -(k_{M\to G} + k_l) \cdot [M] + k_{E\to M} \cdot [E] \#(S2)$$

$$\frac{d[G_\beta]}{dt} = \left(k_{T_1} \cdot P + k_{mw}\right) \cdot [G_\alpha] - \left(k_{T_1} + k_l + k_{mw}\right) \cdot [G_\beta] + k_{E\to G} \cdot \frac{[E]}{2} + k_{M\to G} \cdot \frac{[M]}{2} \#(S3)$$

$$\frac{d[G_\alpha]}{dt} = -\left(k_{T_1} \cdot P + k_l + k_{mw}\right) \cdot [G_\alpha] + \left(k_{T_1} + k_{mw}\right) \cdot [G_\beta] + k_{E\to G} \cdot \frac{[E]}{2} + k_{M\to G} \cdot \frac{[M]}{2} \#(S4)$$

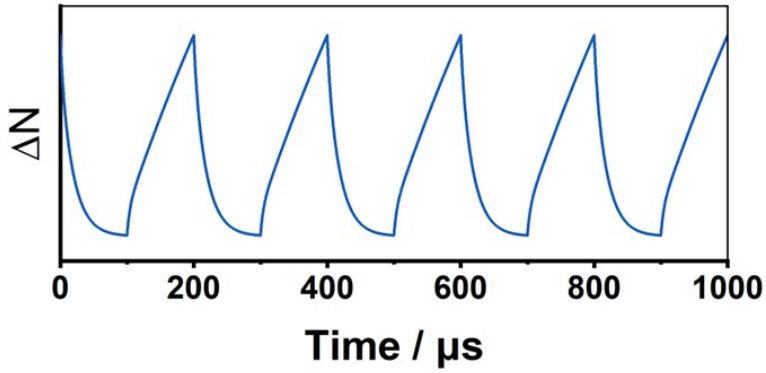

Figure S3. Simulated time-domain signal (ΔN) at 15K, with a modulation frequency of 5 kHz and a duty cycle of 50%.

4. Spin-Lattice Relaxation Time (T_1) Measurements of Ce:YAG at 15 K

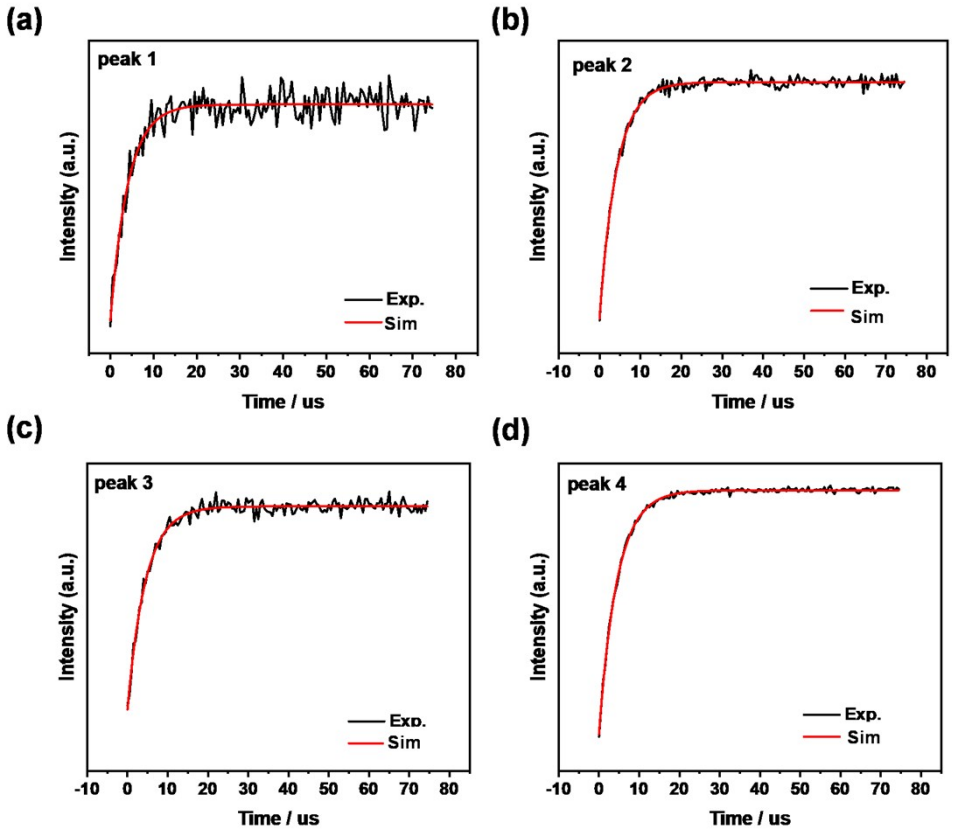

Figure S4. Spin-lattice relaxation time (T_1) for the four resonance peaks of CeYAG measured at 15 K using the inversion recovery pulse sequence (π – T – π/2 – τ – π – τ – echo). (a) Peak 1, (b) Peak 2, (c) Peak 3, (d) Peak 4. The black lines represent experimental data, and the red lines represent simulation results.

Table S1. Simulation results of the T_1 for the four resonance peaks (Peak 1, Peak 2, Peak 3, and Peak 4).

	Peak 1	Peak 2	Peak 3	Peak 4
$T_1/\mu s$	4.06(24)	4.20(7)	4.49(11)	4.53(3)

5.Fluorescence Lifetime of Ce:YAG at 15 K

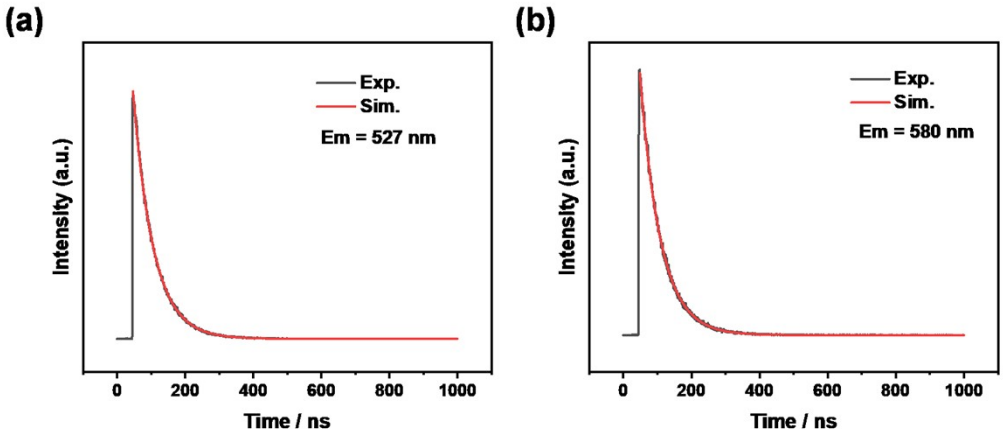

Figure S5. Fluorescence lifetimes of the two emission peaks of CeYAG at 15 K under 445 nm excitation. (a) Emission at 527 nm,$\tau = 60\ ns$. (b) Emission at 580 nm, $\tau = 59\ ns$.

6. The dependence of LIM CW-EPR signal intensity on the laser-on duration for Peak 2

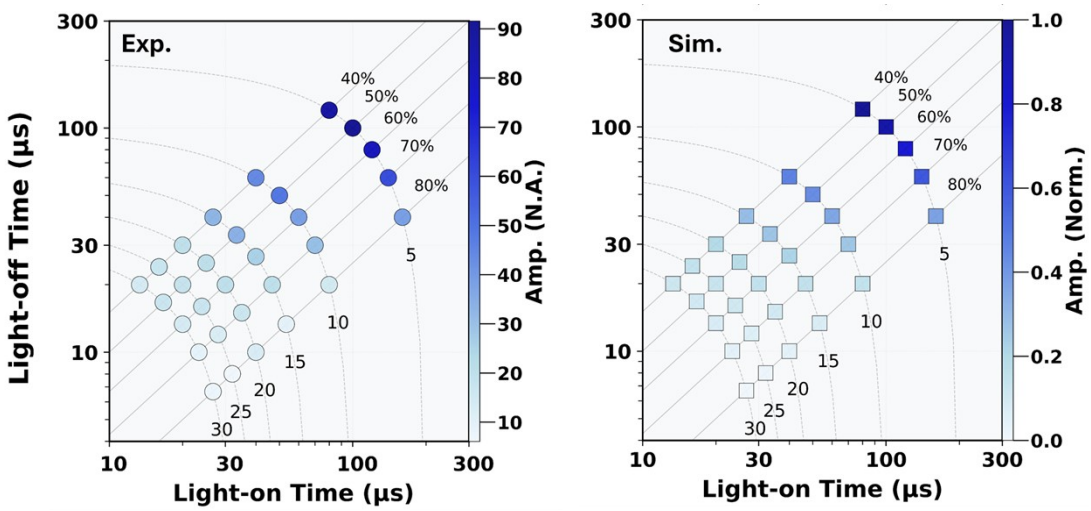

Figure S6. Two-dimensional scatter plots showing the dependence of LIM CW-EPR signal intensity on the laser-on duration (t_{on}) for Peak 2 at 15 K. left: Experimental results. Right: Simulated results based on the model in Figure 2(b).

7. Simulation of the MFM-EPR Spectrum for Yb:YAG

Based on the simulation of the single-crystal rotation spectra of Yb:YAG (Figure S7), we determined that the a-axis of Yb:YAG is parallel to B_0 in the LIM CW-EPR experiment.

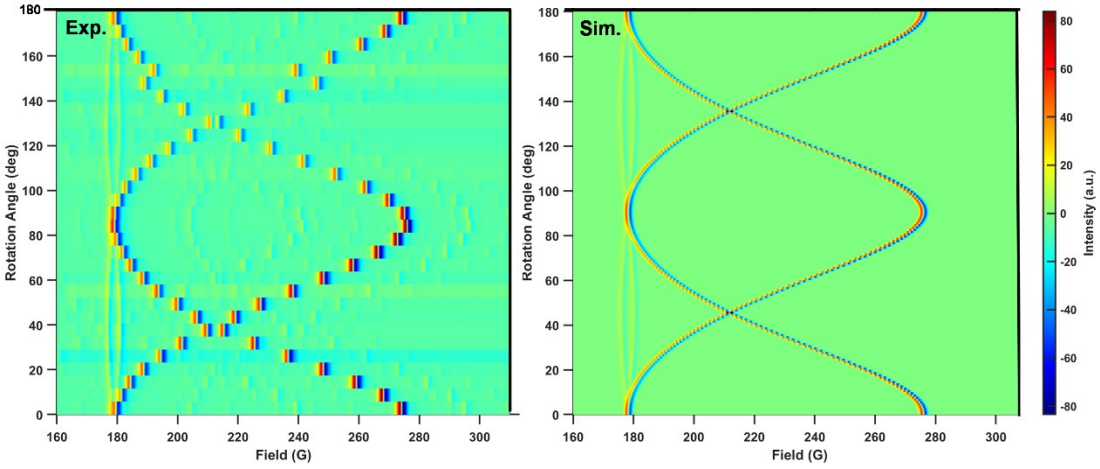

Figure S7. Angle-dependent CW-EPR spectra of Yb : YAG measured at 15 K (left) and the corresponding simulation (right).

8. Room-Temperature Fluorescence Lifetime of Yb:YAG

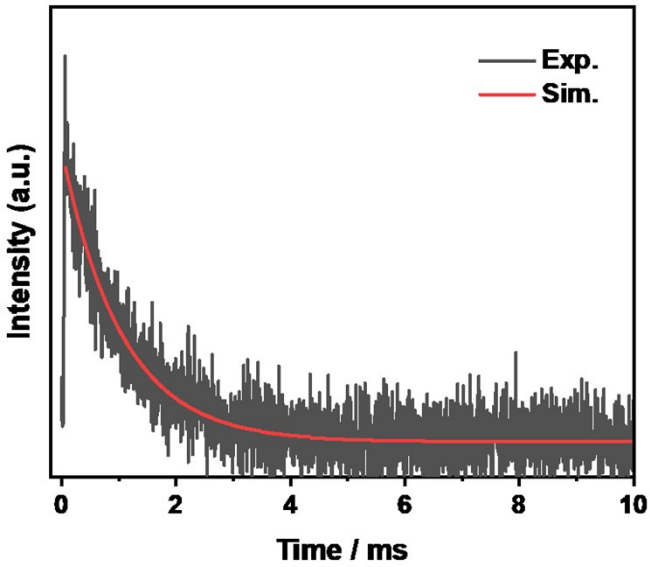

Figure S8. Fluorescence lifetime of the emission peak of Yb:YAG at room temperature under 880 nm excitation, $\tau = 0.93\ ms$.

9. Measurement Parameters for Nd(III), Er(III), and Cr(IV): YAG

Table S2. Measurement Parameters for Nd, Er, and Cr:YAG.

	Nd:YAG	Er:YAG	Cr:YAG
Photoluminescence (PL) Spectra			
Excitation Wavelength	808 nm	808 nm	980 nm
MFM CW-EPR Spectra			
Measurement Temperature	15 K		
Microwave Power/ mW	0.373		
LIM CW-EPR Spectra			
Measurement Temperature	15 K		
Microwave Power/ mW	1.49	23.8	1.49
Laser Power/ mW	50		
Modulation Frequency/ kHz	5	5	1
Duty cycle	50%		